Flow patterns in an occluded artery with an "end to side" anastomosis model. A visualisation study

I. D. Kalogirou, A. Romeos, A. Giannadakis, , K. Perrakis, T. Panidis

***Abstract*—** The hemodynamic field of an occluded artery with a 45^o distal 'end to side' anastomosis is examined experimentally. The influence of the host and graft vessel inlet conditions on the junction region flow dynamics are discussed, via a visualisation approach. A thin sheet of laser light, illuminating various sections along the test model, was used to analyse the local structure attained in the junction area, as well as in the proximal and distal regions of the merging section. In this study both the steady and pulsatile flow cases are considered. The qualitative description is obtained in a range of Reynolds and Womersley numbers typically occurring in human cardiovascular systems. Emphasis is placed on the detection of regions susceptible to deterioration of the bypass system performance associated in principle with swirl and backflow motion. The rearrangement of the hemodynamic field downstream of the anastomosis and its sensitivity to the merging host and graft stream conditions is an issue of particular interest here, also.

***Keywords*—** Biofluids, Anastomosis, Stenosis, Hemodynamics

I. Introduction

THE cardiovascular system primary function is the transport of nutrient and waste throughout the body. The heart pumps blood through a sophisticated network of branching tubes. The arteries, far from inert tubes, adapt to varying flow and pressure conditions by enlarging or shrinking to meet changing hemodynamic demands. The typical Reynolds number range of blood flow in the body varies from 1 in small arterioles to approximately 4000 in the largest artery, the aorta. Thus the flow spans a range in which viscous forces are dominant on one end and inertial forces are more important on the other [1].

Atherosclerosis is a critical cardiovascular disease, characterized by the deposition of atheromatous plaques containing cholesterol and lipids on a layer on the inner walls of the large and medium-sized arteries, resulting in a reduction in the cross-sectional area of the vessel lumen and an impeded or blocked blood flow [2]-[4]. The phenomenon of atherosclerosis has been recognised as one of the most severe arterial diseases as it can lead to stenosis of arteries and consequently to heart or brain stroke.

The bypassing of critically stenosed arteries (>75%), using either an autologous vein or prosthetic graft, is a common surgical procedure. Various schemes of artery bypassing methods have been adopted by the Surgeons' community such as "end to side" or "side to side" anastomosis, sequential anastomosis, Π or Y graft anastomosis etc [5], [6].

Unfortunately, bypass graft implantation failure is a common postoperative problem. The development of anastomotic Intimal Hyperplasia (IH) is a principal factor for vessel pathogenesis and accounts for approximately 25% fail in one year and about 50% in ten years [7]. This abnormal, progressive thickening of the layer of the artery inner wall is prominent at the heel, toe and along the suture line where the graft is fixed to the recipient vessel, and on the artery floor opposite the junction. Intimal hyperplasia causes the gradual narrowing of the vessel lumen, and is a major factor responsible for bypass graft failure.

Various hypotheses on the influence of local hemodynamics have been presented in the literature. In particular, the theories that are based on the influence of low or oscillating wall shear stresses at or near the anastomoses have gained attention. Several researchers [9]-[13] have shown that low shear stress and oscillating shear forces at the arterial floor and the heel, plus a high Wall Shear Stress (WSS) gradient at the toe probably promote IH development. These phenomena have been also correlated with the presence of flow separation causing vortex formation, flow recirculation, and flow stagnation at the region of anastomosis and especially where pathologic studies have reported discrete development of IH, denoting that the configuration of an anastomosis may be a factor in the localization of Intimal Hyperplasia.

The work presented below is focusing to the case of "end to side anastomosis", where there are still open issues regarding the understanding of the interaction of the vortical structure,

November 30, 2015. This work was supported by the TEI of Western Greece's "EPEAEK-ARXIMIDIS III" Research Program., financed by The European Union & the Ministry of Education, Lifelong Learning and Religious Affairs of Greece.

I.D. Kalogirou is with the Laboratory of Fluid Mechanics, Department of Mechanical Engineering, TEI of Western Greece, (e-mail: kalogirou@teiwest.gr)

A. Romeos is with the Laboratory of Fluid Mechanics, Department of Mechanical Engineering, TEI of Western Greece, (e-mail: alekosromeos@gmail.com)

A. Giannadakis is with the Laboratory of Fluid Mechanics, Department of Mechanical Engineering, TEI of Western Greece, (e-mail: ngiannad@gmail.com)

K. Perrakis is with the Laboratory of Applied Thermodynamics, Department of Mechanical Engineering and Aeronautics, University of Patras (e-mail: perrakis@mech.upatras.gr)

T. Panidis is with the Laboratory of Applied Thermodynamics, Department of Mechanical Engineering and Aeronautics, University of Patras (e-mail: panidis@mech.upatras.gr).

formed due to arterial stenosis with a bypass graft and is part of an ongoing research held in Laboratory of Applied Thermodynamics, University of Patras and the Laboratory of Fluid Mechanics, TEI of Western Greece [14]-[17].

II. Experimental Procedure

A. Experimental Configuration

The details of the experimental configuration are depicted in Fig. 1. Two major flow lines co-exist, so that the experimental model of the stenosis and the anastomosis can be studied under steady (straight line) or pulsatile (dash & dash dot lines) flow conditions. Pressure and flow stabilisation are achieved through a combination of reservoirs and tanks, shown in Fig.1. Flow distribution and regulation are imposed through ball valves, while flow rate measurement is implemented through a Rotameter (steady flow) or Electromagnetic Flow Meters attached to the stenosis and anastomosis flow line (pulsatile flow). For the case of the steady flow, mass flow distribution between the stenosis and anastomosis flow line is accounted for via the continuity equation.

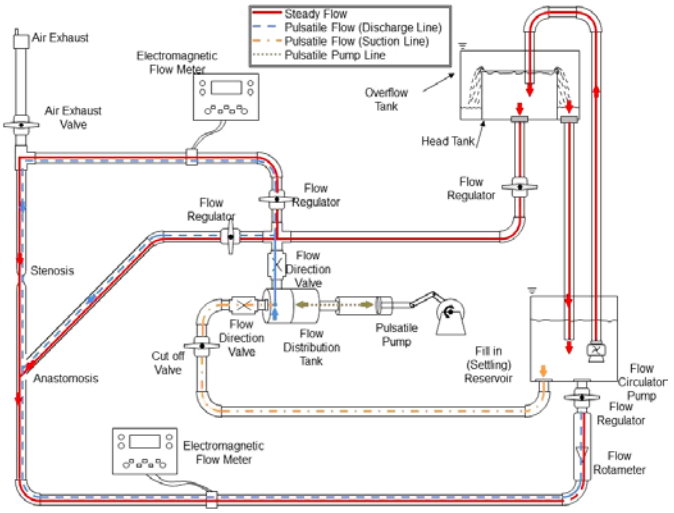

Fig.1 Experimental Apparatus Schematic

As shown in Fig. 2 the artery model under consideration is constructed by Plexiglas material that is internally machined so that index matching is achieved (the working fluid consisting of a water-glycerin mixture has a refractive index close to that of the Plexiglas), and that light difraction is decreased. Both the artery and the anastomosis models' inner diameters (tube, D) are 24 mm, while the stenosis' inner diameter (contraction, d) is 12 mm. The occlusion of the "artery model" is 75%, while the angle of insertion for the anastomotic "graft model" is 45°.

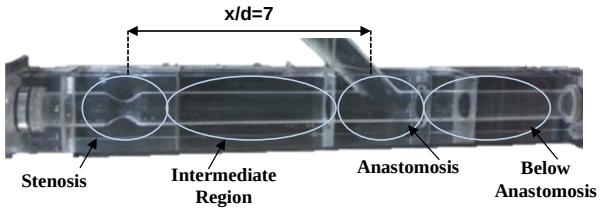

Fig.2 Experimental Configuration Design

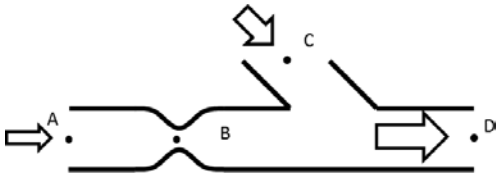

Fig. 3 Flow Configuration Schematic

B. Experimental Approach of Blood Flow

A water-glycerine mixture (55%-45%) with a dynamic viscosity similar to that of blood (μ=3.5cP) is used as the flow medium attaining similar Reynolds numbers with the modelled flow.

As the cyclic nature of the heart pump creates pulsatile conditions in all arteries, a piston driven diaphragmatic pump (Fig.4) is used to simulate heart's systolic and diastolic cycle as shown in Fig. 5. The piston's movement is controlled via a peripheral, software based, automation system simulating the heart flow cycle characteristics. As seen in this figure, the unsteady flow situation is simulated by a pulse waveform that is typical to femoral and iliac arteries, rather than the coronary one [14].

Fig.4 Pulsatile Pump

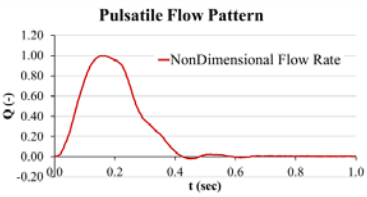

Fig. 5 Heart Cycle Simulation

C. Visualisation Technique

The visualisation of the model artery flow field was carried out by making screenshots at various successive positions along the model, as indicated in Fig. 2. The visualisation technique used was the laser sheet illumination method. A thin sheet of laser light illuminated the symmetry plane of the observation region which extended from the tube just upstream of the stenosis, to the tube immediately downstream anastomosis. Hollow glass spherical particles with mean diameter <150 μm were used as seeding material for capturing characteristic coherent structure and flow trajectory patterns. A variety of digital cameras operating at appropriate to the investigated flow attribute shutter speeds and apertures were used, to elucidate local structure. The flow rate ratio of the stenosis/anastomosis balance was specified as 35% to 65% of the total flow rate, respectively.

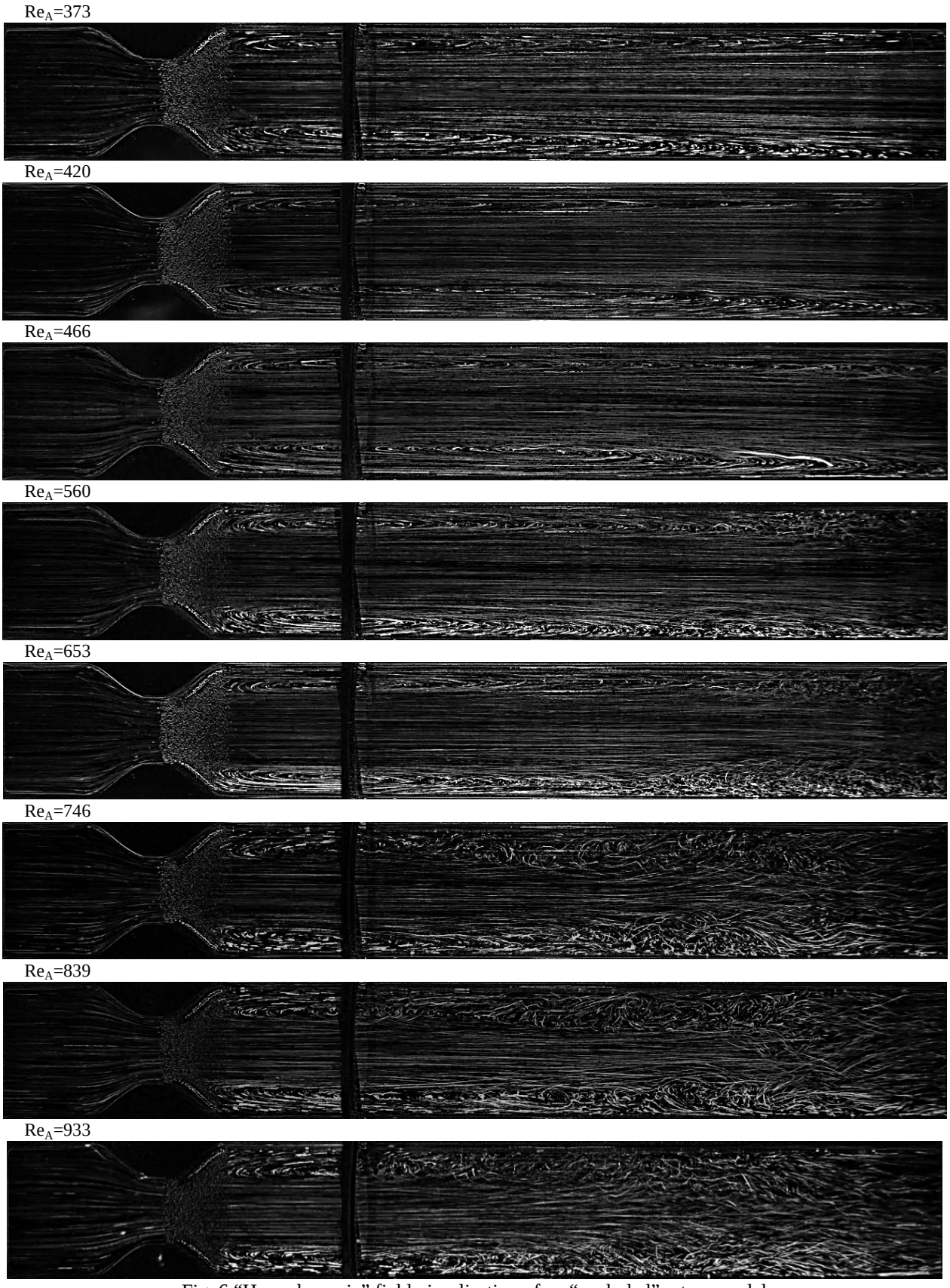

Fig. 6 “Hemodynamic” field visualisation of an “occluded” artery model

A. Inlet Flow Conditions

Although the original flow in the cardiovascular system of living organisms is pulsatile, it is quite common to study steady state relevant flow configurations as well. Many experimental and computational works rely on steady flow results, obtained in artery models with fluid mediums that are either Newtonian or non-Newtonian, in order to get a perception of the original, time dependent flow dynamics. Clearly, the steady state structure is quite similar to the pulsed situation, especially in the acceleration (systolic) phase of the latter. This practice is followed in the present study, where both configurations are studied successively. Steady flow results are presented in the following, without and with an anastomosis in the occluded artery model.

The "hemodynamic" field of the occluded "artery" model (no anastomosis present) is investigated for eight different Reynolds numbers varying from Re_A=373-933 for the case under steady flow conditions.

With the presence of the anastomosis, two Reynolds numbers Re_D= 1007 and Re_D=3183, respectively, are considered for steady flow conditions. Reynolds number is calculated with respect to the total mass flow rate by applying the continuity equation at point D as shown in Fig.3.

Visualisation study of the pulsatile flow case is performed by setting the total duration of the cycle to approximately 1 sec, corresponding to 60 heartbeats per minute or a supply rate of 60 cm^3/cycle. The above inflow conditions correspond to the higher supply flow rate (Re_D=3183) of the steady flow case. The corresponding Womersley number is 30.

III. Results and Discussion

A. "Hemodynamic" Field of the Occluded "Artery" Model as a Function of Reynolds Number

The main objective here is the discussion of the complex interaction field occurring in the mixing region of the flow evolving downstream of the stenosis and the bypass stream ejected in the anastomosis region. However, a better appreciation of the complicated nature of the flow regime established in the merging section of the above streams can be gained by examining the stenosis configuration in the absence of anastomosis first.

Fig.6 presents the flow patterns attained in the region immediately after the contraction of the stenosis, extending up to approximately 12 contraction diameters, d, (6 tube diameters, D) downstream as a function of Reynolds number. The x/D = 0 position is located at the minimal cross section of the contraction. The Reynolds numbers indicated in the figure are based on the tube diameter (upstream or downstream of the contraction) and cover the range 373 – 933. Clearly, a confined jet flow issuing from the contraction is seen to interact with swirling motions located along the tube walls in all images presented. The near wall (upper and lower) recirculating regions originate in the diverging section of the stenosis due to boundary layer separation caused by an adverse pressure gradient prevailing in this section.

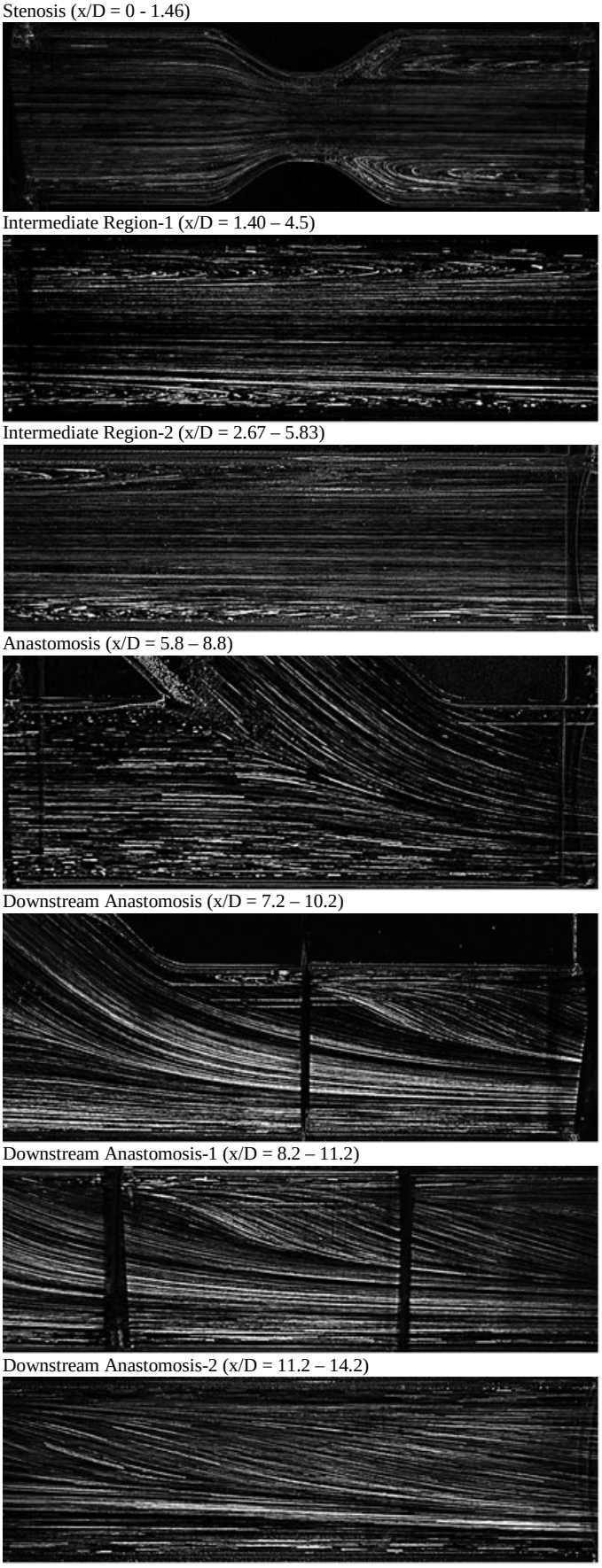

Fig. 7 Visualisation of a bypassed "occluded" artery for Re_D=1007

The vorticity of each recirculating bubble has the same sign as that of the corresponding boundary layer over which it develops, i.e. counter clockwise and clockwise rotation in the upper and bottom duct wall respectively. However, the streamwise extent of the near wall recirculating areas decreases with increasing Reynolds number. It ranges from approximately 6D at Re=373, to approximately 2D at Re=933, suggesting an inverse proportionality between recirculation length and Reynolds number attained. Beyond those distances, recirculating bubble fluid is shed in the flow direction, the near wall swirling motion becomes diffused and mixes with the core jet flow. The mixing of the near wall recirculation zone with the initially irrotational core flow becomes more intense and is apparent in the presented images, as the Reynolds number increases. The lateral extent of the mixing patterns due to entrainment of near wall fluid into the core zone increases with Reynolds number. At the same time, the central "irrotational" region diminishes in length. Within the 6D region of observation in the presented photographs (just 1D ahead the anastomosis, located at 7D in the subsequent experiments), a qualitatively different in character flow approaches the merging region with varying Reynolds number. From the relatively "unmixed" strongly inhomogeneous situation at Re=373, to an intensely mixed far more homogeneous, (compared to the low Re case), flow configuration at Re=933.

It is evident from the above discussion, carried out in the absence of the additional complexity imposed by a bypass emerging stream, that the graft should not be implanted immediately after the stenosis. A more distal to the contraction implantation could possibly prevent, or at least minimise undesirable recirculating motion at the heel which in turn could lead to hyperplasia at this location.

B. "Hemodynamic" Field of a Bypassed "Occluded" Artery with an "End to Side" Anastomosis: The "Steady Flow" Case

In this section a discussion is carried out regarding the development of the flow field for the case that the occluded "artery model" is by-passed with an "end to side" anastomotic "graft". Qualitative results of the "hemodynamic" field are presented for two Reynolds numbers based on the merging flow characteristics after the anastomosis and the duct diameter, D, under steady inlet flow conditions. The low Reynolds number case (Re_D=1007 presented in Fig.7) corresponds to Re_A=353 for the inlet flow conditions prevailing upstream of the stenosis.

This configuration is quite close to the Re_A=373 case discussed in the previous section. Similarly, the high Re case (Re_D=3183 in Fig.9) corresponds to Re_A=1114 inlet condition, close to the high Re case (Re_A=933) of the occluded artery of the previous section.

The low Re case depicted in Fig. 7 exhibits identical overall signature regarding the flow approaching to the anastomosis region with the low Re occluded situation of the previous case in the absence of anastomosis. This indicates that the emerging graft flow seems to have no upstream effects.

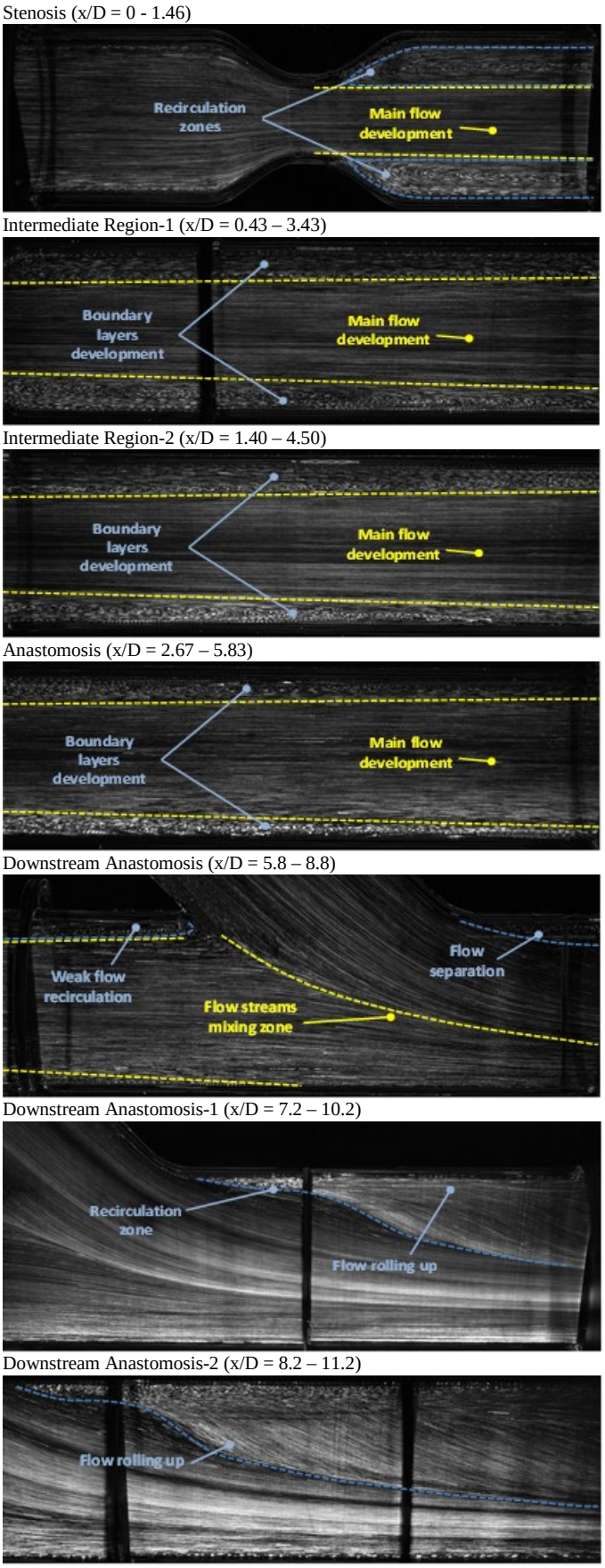

Fig. 8 Standard deviation of the instantaneous snapshots for low Reynolds case, Re_D=1007

Stenosis (x/D = 0 – 2.3)

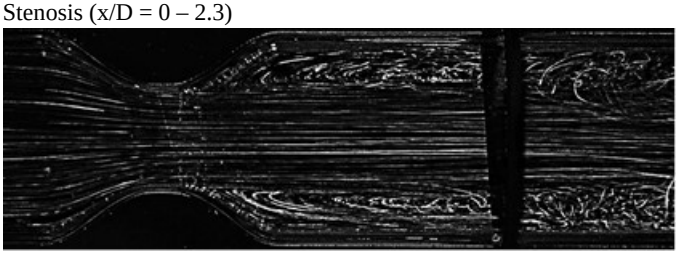

Downstream Stenosis (x/D = 0.3 – 3.26)

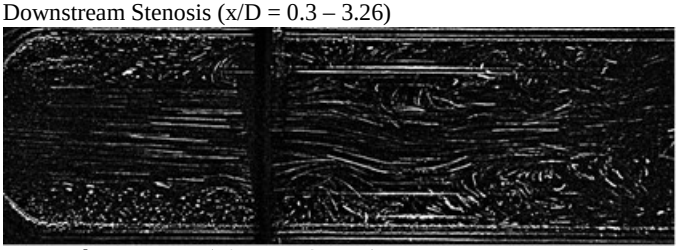

Intermediate Region (x/D = 1.46 – 4.4)

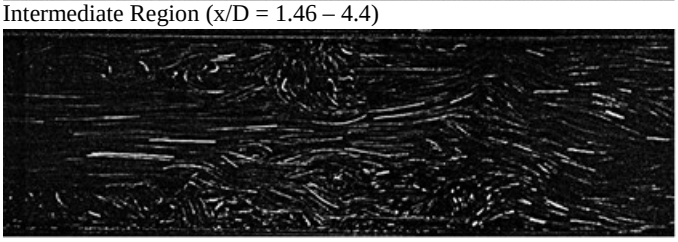

Intermediate Region (x/D = 4.14 – 7.1)

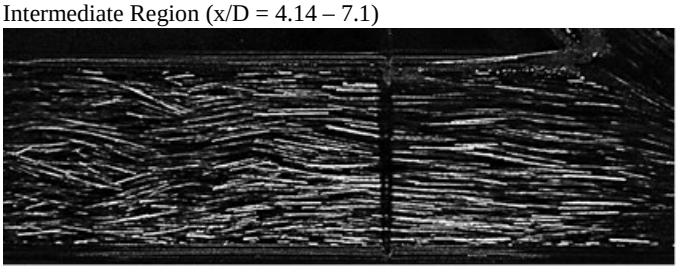

Anastomosis (x/D = 5.9 – 8.8)

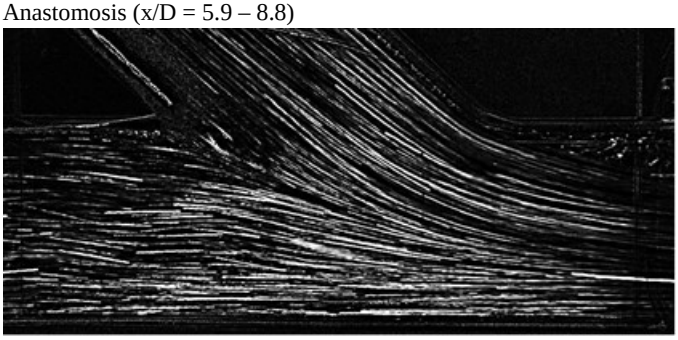

Downstream Anastomosis (x/D = 7.2 – 10.16)

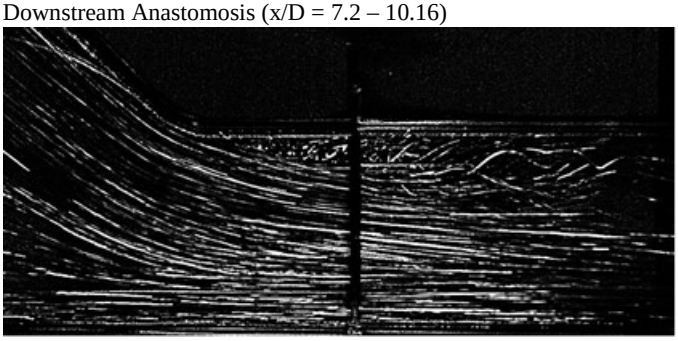

Fig. 9 Visualisation of a bypassed "occluded" artery for Re_D=3183

A small recirculation area with streamwise extent ~0.8D is observed at the anastomosis heel, as a result of the duct upper boundary layer blockage produced by the incoming graft fluid. Flow separation and reversal occurs on the opposite side of the anastomosis graft, at the toe region. The axial velocities are higher in the lower half of the main tube, as seen in the last four photos of Fig. 7, in a manner similar to that found when a developed flow enters a curved bend.

Fig. 8 presents results obtained from statistical analysis processing of the instantaneous snapshots shown in Fig. 7 for the low Re case. The standard deviation of numerous observations taken at each particular x/D range has been derived and presented in this figure. This demonstration allows clarifying individual regions, (as well as their extent), where a certain type of coherent motion prevails. The boundaries of the confined jet and the surrounding wall flow in the proximal to graft region, as well as their weak interaction, can be more sharply identified in the processed representation. A weak flow recirculation motion is also observed at the heel region. In the junction section, the acceleration of the flow in the near bed (bottom wall) region, as a result of merging of the confined jet and the impinging graft flow is clearly qualitatively envisaged. Velocity maxima accompanied with steep transverse velocity gradients and therefore increased shearing action take place in the near bed zone of the junction and along its distal direction. Flow separation and reversal is observed at the toe, an unwanted effect that could lead to material deposition and possible graft failure in this region. Intense descending motion, especially 1D after the toe tip in the upper host vessel zone, is clearly observable at the last downstream sections of Fig. 8. As noted before, the central azimuthal plane of the artery-graft model is illuminated here. Hence, only the downward motion of the central plane flow can be viewed in the photographs. In this region, a pair of counter rotating secondary vortices, symmetrical to the central plane, is developed due to cross stream pressure gradients leading to crescent like axial velocity distributions. The locus of the vertical span of the secondary recirculating area is indicated in Fig. 8.

A far more homogeneous flow approaches the graft mixing region for the high Re case (Re_D=3183), presented in Fig. 9. In this case, it is hard to distinguish and unambiguously, clarify (as far as the visualisation technique allows), the existence of a recirculation zone at the heel region. Flow separation is more intense at the toe and the separated motion proceeds deeper into the core flow region than in the low Re case. Also, the high momentum inlet graft flow penetrates deeper the weak mainstream flow in this configuration as the axial velocity streakline lengths indicate.

Fig. 10 presents the standard deviation of the instantaneous events depicted in Fig. 9. A far more intensely mixed than the low Re situation proximal flow enters the junction section. The deeper penetration of the graft flow in the host duct bed region, as well as the more diffuse and turbulent character of the separated at the toe flow and the subsequent secondary roll up region, are quite evident in this figure.

Stenosis (x/D = 0 – 2.3)

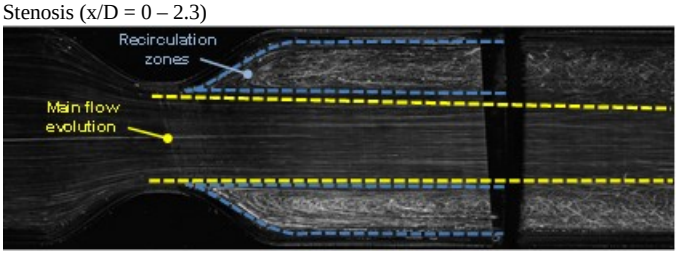

Downstream Stenosis (x/D = 0.3 – 3.26)

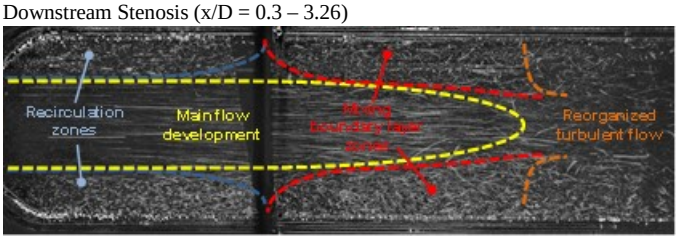

Intermediate Region (x/D = 1.46 – 4.4)

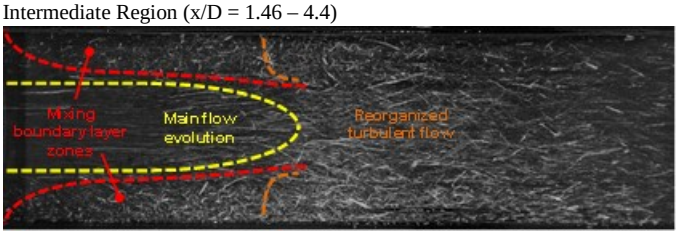

Intermediate Region (x/D = 4.14 – 7.1)

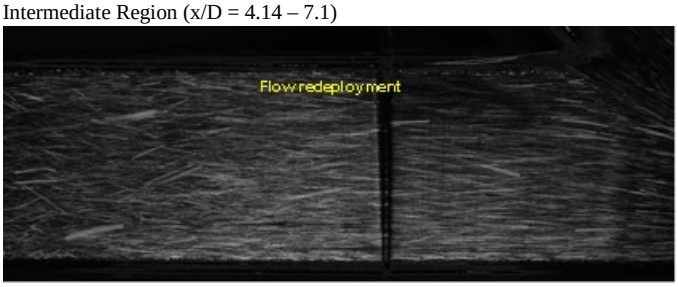

Anastomosis (x/D = 5.9 – 8.8)

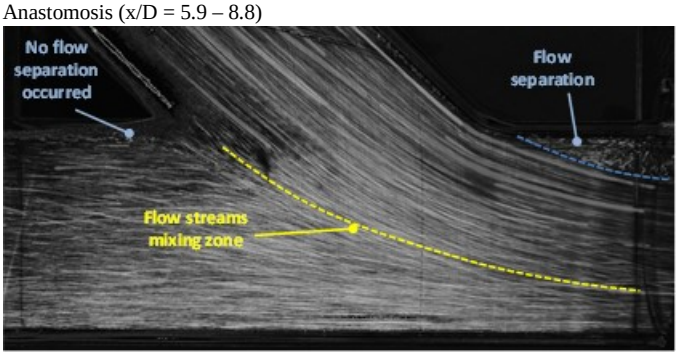

Downstream Anastomosis (x/D = 7.2 - 10.16)

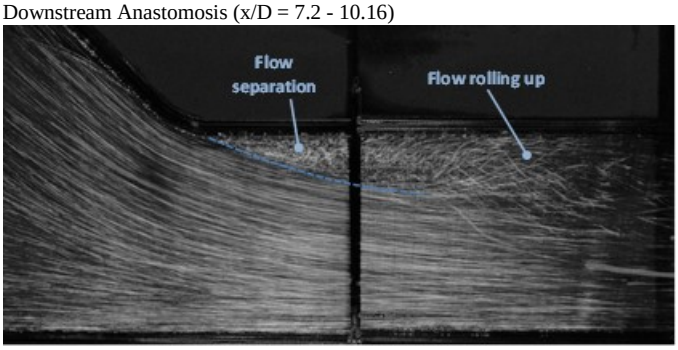

Fig. 10 Standard deviation of the instantaneous snapshots for high Reynolds case, Re_D=3183.

C. "Hemodynamic" Field of a Bypassed "Occluded" Artery with an "End to Side" Anastomosis: The "Pulsatile Flow" Case

The "hemodynamic" field's visualisation study of a bypassed "occluded" artery with an "end to side" anastomosis is discussed below for two characteristic instants of blood flow cycle: (a) maximum discharge flow rate (systolic) phase and (b) reversal (diastolic) phase. As shown in Fig. 5, these two instants correspond to the maximum flow rate (0.1 - 0.2 sec) and the reversal of flow (0.4 - 0.6 sec).

During phase (a) presented in Fig. 11, strong axial motion is observed throughout the "artery" model, while secondary radial motions are observed near the walls. These secondary motions extend for about 3.0D downstream the stenosis, while strong mixing with the central jet – like motion occurs at about 3.5D downstream the stenosis in the streamwise direction. From this point downstream, flow in the artery model becomes turbulent reaching the anastomosis "heel" by having acquired fully developed flow characteristics. Flow coming from the artery model is being forced to follow the trajectory of the one entering from the "anastomotic graft" due to the significantly higher momentum. Small corner effects are observed at the "heel" of the anastomosis, where a backflow motion appears. Secondary motions reappear at the "toe" of the anastomosis and extend for about 3.5D in the streamwise direction (near the wall of the artery model), where backflow movements are apparent. The overall picture of the acceleration – systolic phase of the pulsed flow shows close resemblance to the high Re steady case, previously discussed.

Backflow motion and flow recirculation trends are the main characteristic of the presented instant of the diastolic phase (b) as it is depicted in Fig. 12. Wide and spreading recirculation zones appear at the upstream side of the stenosis, while the whole of the artery model's volume is occupied by secondary vortical structures.

A characteristic feature of the diastolic phase is the fact that the recirculating structures formed downstream of the anastomosis, during the systolic phase, have moved upstream, forming a wide vortex that covers almost the whole of the anastomosis's cross sectional area, an observation similar to that made by Hughes and How [18].

IV. Conclusions

A visualization study has been carried out in an occluded artery with an end to side anastomosis model. Steady and pulsatile flow conditions were considered in a range of Reynolds and Womersley numbers typically encountered in human cardiovascular systems. The resulting mixing configuration in the anastomosis region, (recirculation strength and spatial extent and graft flow penetration depth in the host vessel), is affected by the host artery flow conditions and distance of the junction from the contraction. The qualitative description indicates the heel and toe regions as the most prominent locations for intimal thickening both for the steady and the unsteady flow cases and the whole Reynolds and Womersley number range studied.

Stenosis

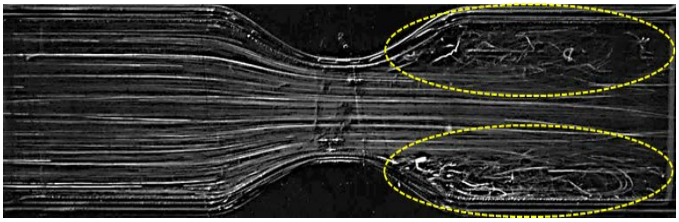

Downstream Stenosis

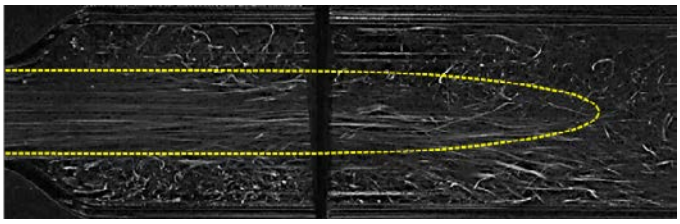

Far field downstream stenosis

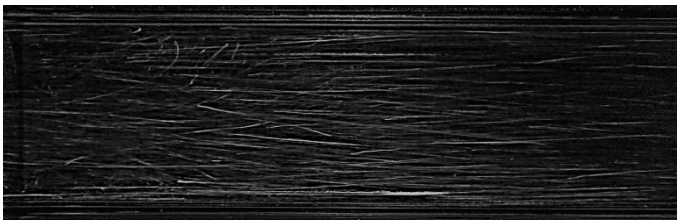

Near upstream field of the anastomosis

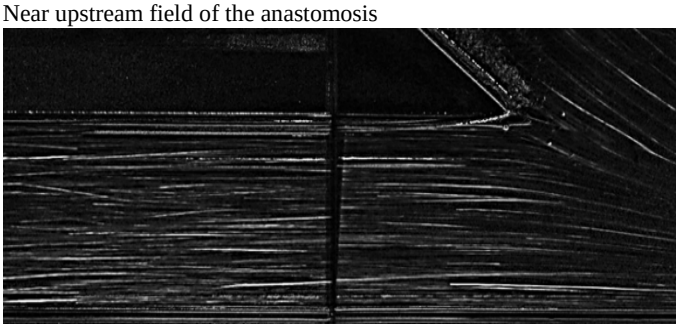

Anastomosis

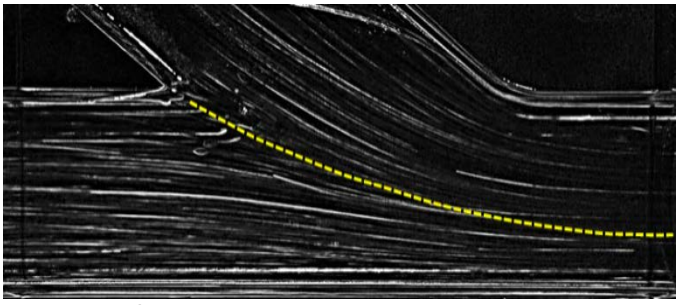

Downstream Anastomosis

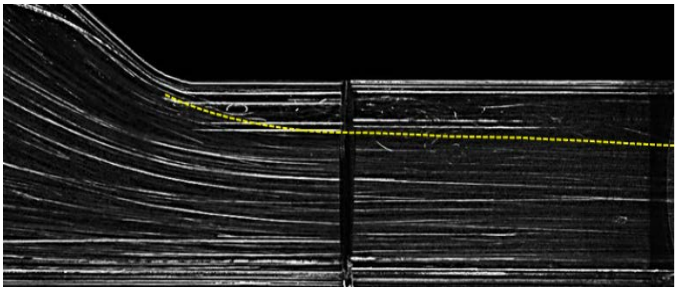

Fig. 11 Visualisation of a bypassed “occluded” artery W=30 (Systolic Phase)

Stenosis

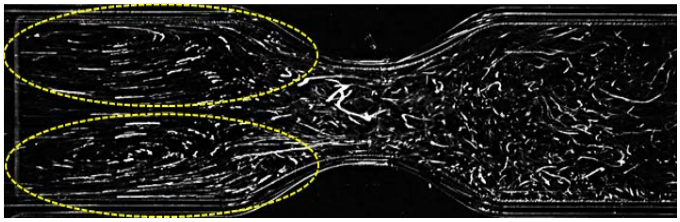

Downstream Stenosis

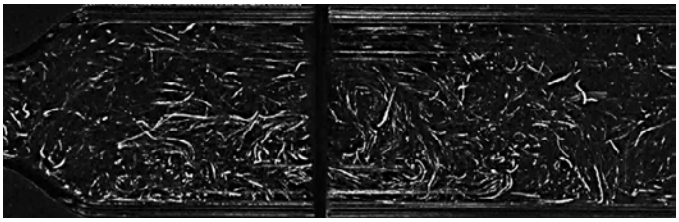

Far field downstream stenosis

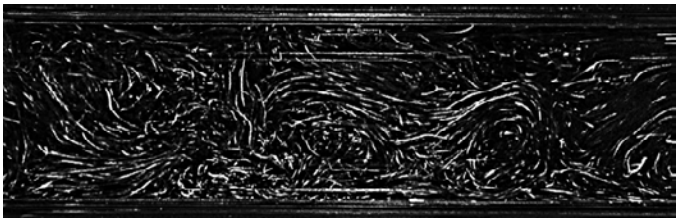

Near upstream field of the anastomosis

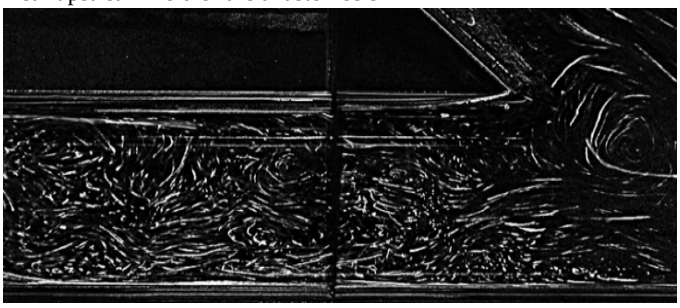

Anastomosis

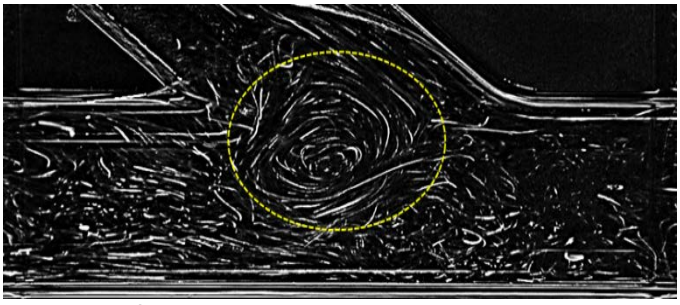

Downstream Anastomosis

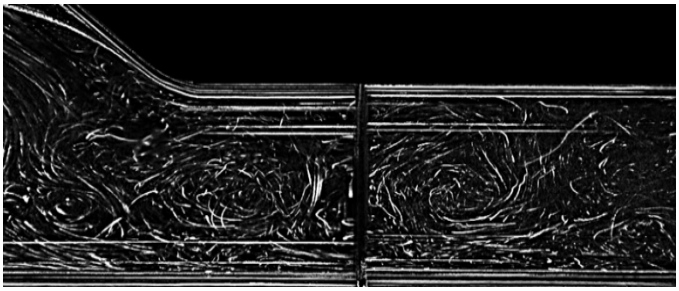

Fig. 12 Visualisation of a bypassed “occluded” artery W=30 (Diastolic Phase)

In the pulsatile mode, the acceleration phase flow dynamics is quite similar to that of the high Re steady situation. The main characteristics of the diastolic phase flow configuration are backflow motion and flow recirculation in an overall low velocity environment. Thus, the deceleration phase flow regime is more amenable to IH development than that of the systolic counterpart.

REFERENCES

[1] N. David Ku, "Blood Flow in Arteries", Annu. Rev. Fluid Mech., 1997, Vol.29 , pp. 399–434,

[2] Q. Aike., L. Youjun, L. Siyang, Z. Hu, "Numerical Simulation of Physiological Blood Flow in 2-way Coronary Artery Bypass Grafts", J. Biological Physics, 2005, Vol. 31: 161-182H. Poor, *An Introduction to Signal Detection and Estimation*. New York: Springer-Verlag, 1985, ch. 4.

[3] B. Nuntadilok, B. Wiwatanapataphee, M. Chuedoung and T. Siriapisith, Numerical simulation of blood flow in the system of human coronary arteries with and without bypass graft, Proc. 11th WSEAS Int. Conf. on System Science and Simulation in Engineering, Singapore, (2012), 43-48

[4] P. Chuchard, T. Puapansawat, T. Siriapisith and B. Wiwatanapataphee, Numerical simulation of blood flow in the system of human coronary arteries with stenosis, Proc. 4th WSEAS Int. Conf. on Finite Differences Finite Elements Finite Volumes Boundary Elements, France, (2011), 59-63

[5] Loth F., Fischer P.F., Bassiouny H.S., 2008, "Blood Flow in End to Side Anastomosis", Annu. Rev. Fluid Mech., Vol.40: 367-393

[6] Bassiouny H.S., White S., Glagov S., Choi E., Giddens D.P., Zarins C.K., 1992, "Anastomotic intimal hyperplasia: mechanical injury or flow induced", J. Vasc. Surg. Vol. 15:708–16

[7] Giordana S, Sherwin SJ, Peiro J, Doorly DJ, Crane JS, et al. 2005. "Local and global geometric influence on steady flow in distal anastomoses of peripheral bypass grafts". J. Biomech. Eng., Vol. 127:1087–9

[8] Keynton RS, Evancho MM, Sims RL, Rodway NV, Gobin A, Rittgers SE., 2001, "Intimal hyperplasia and wall shear in arterial bypass graft distal anastomoses: an in vivo model study", J. Biomech. Eng., Vol. 123:464–7

[9] Kohler TR, Kirkman TR, Kraiss LW, Zierler BK, Clowes AW, 1991, "Increased blood flow inhibits neointimal hyperplasia in endothelialized vascular grafts", Circ. Res., Vol. 69:1557–65

[10] Loth, F., Jones, S.A., Zarins, C.K., Giddens, D.P., Nassar, R.F., Glagov, S. and Bassiouny, H.S., 2002, "Relative Contribution of Wall Shear Stress and Injury in Experimental Intimal Thickening at PTFE End-to-Side Arterial Anastomoses", J. Biomech. Eng., Vol.124: 44–51

[11] Politis A.K., Stavropoulos G.P., Christolis M.N., Panagopoulos P.G., Vlachos N.S., Markatos N.C., 2008, "Numerical modelling of simulated blood flow in idealized composite arterial coronary grafts: Transient flow", Journal of Biomechanics, Vol.41(1): 25-39

[12] Politis A.K., Stavropoulos G.P., Christolis M.N., Panagopoulos P.G., Vlachos N.S., Markatos N.C, 2007, "Numerical modeling of simulated blood flow in idealized composite arterial coronary grafts: Steady state simulations", Journal of Biomechanics, Vol. 40(5):1125-1136

[13] C. Ross Ethier, D.A. Steinman, X. Zhang, S.R. Karpik, M. Ojha, 1998,, "Flow waveform effects on end-to-side anastomotic flow patterns", Journal of Biomechanics, Vol.31: 609-617

[14] A. Giannadakis, K. Perrakis, E. Apostolakis, D. Mavrilas, "Experimental and numerical investigation of the flow field in a model of human arteries (the double stenosis case)", AERC 2006, 3rd Annual European Rheology Conference, April 27-29, Hersonisos – Crete, 2006

[15] A. Giannadakis, D. Mavrilas, E. Apostolakis, K. Perrakis, "An approach to study the flow field in a model of sequential stenosed human arteries", Fifth World Congress of Biomechanics - Munich 2006

[16] A. Giannadakis, K. Perrakis, T. Panidis, A. Romeos, "Experimental Investigation of the Hemodynamic Field of Occluded Arteries with Double Stenosis", 10th International Workshop on Biomedical Engineering, October 5-7, Kos- Greece, 2011

[17] A. Romeos, A. Giannadakis, I. Kalogirou, K. Perrakis, Th. Panidis, "Visualization study of an occluded artery with an end to side anastomosis", CSCC/INASE, 19th International Conference, Zakynthos Island Greece, July 16-20, 2015

[18] Hughes, P.E., How, T.V, 1996, "Effects of Geometry and Flow Division on Flow Structures in Models of the Distal End-to-Side Anastomosis", Journal of Biomechanics, Vol.29 (7): 855-872